First principles molecular dynamics study of amorphous $Al_xGa_{1-x}N$ alloys

Kuiying Chen[a] and David A. Drabold
Department of Physics and Astronomy, Ohio University, Athens, Ohio 45701

(Received 18 April 2001; accepted for publication 25 March 2002)

We have systematically investigated atomic structures, electronic and dynamical properties of amorphous aluminum–gallium–nitride alloys (a-AlGaN) by performing first principles local basis molecular dynamics simulations. The network topology and defects of the amorphous 216-atom model system have been analyzed with the radial distribution function, the angular distribution function, the ring statistics, and the local coordination. It was found that the models have mixed threefold and fourfold coordinations, and the number of threefold (fourfold) coordinated atoms in alloys decreased (increased) with increasing Al composition. No odd rings are found, indicating that no wrong bonds (homonuclear bonds) appear in the a-$Al_xGa_{1-x}N$ alloys. The Ga–N and Al–N bond lengths show a small variation with the Al composition, which is in agreement with recent extended x-ray absorption fine structure experimental measurements. The electronic properties examined by the electronic density of states and local bonding character demonstrate that no mid-band-gap states exist. The band-gap dependence on Al fraction x in a-$Al_xGa_{1-x}N$ alloys shows a nearly linear variation with Al composition, and exhibits a small downward bowing behavior. It was also shown that valence band tail states are mostly localized on the threefold coordinated N sites, while the conduction band tail states are mostly localized on the threefold coordinated Ga and Al sites, and the electronic localization tends to become weaker with the addition of Al. We find a mixture of sp^3 and sp^2 bonds present in the network and their interaction plays a key role in the dynamical properties of a-$Al_xGa_{1-x}N$ alloys. © *2002 American Institute of Physics.*
[DOI: 10.1063/1.1478132]

I. INTRODUCTION

The wide-energy gap III–V nitride semiconductors GaN and AlN have received considerable attention in both experiment[1–8] and theory[9–13] for their device applications in blue and ultraviolet wavelengths. The majority of research on III–V nitrides has been focused on the wurtzite and zinc-blende crystal phases. To provide a basis for understanding future wide-energy gap device concepts and applications based on wurtzite and zinc-blende III–V nitride, first principles investigations for $Al_xGa_{1-x}N$ alloys have been performed.[14–17] The crystalline AlGaN alloys grown by metalorganic chemical vapor deposition (MOCVD) are known to have a nearly linear relationship in composition versus band gap with values ranging between 3.42 eV for GaN and 6.2 eV for AlN.[18,19] Recently, amorphous AlN, GaN, and AlGaN alloys have been grown using reactive sputtering.[20] Surprisingly, the electronic density of state of amorphous AlGaN alloys, like their crystalline counterparts, exhibits no midgap defect state.[20] The band gap exhibits a nearly linear growth with Al concentration.

Rare-earth-doped amorphous aluminum–gallium–nitride alloys are of high practical importance because they can be stimulated to emit blue and ultraviolet light, and the band-gap composition will determine the color of light emitted from devices constructed with these materials. Finally, these materials have special advantages, such as a natural tendency to a state free gap without hydrogeneration, and are therefore potentially useful as hosts for optically active dopants and possibly for electronic purpose.

Although there are first principles calculations of crystalline and *random* AlGaN alloys,[21] there has been so far no *realistic* large scale calculations of a-AlGaN alloys that support the band-gap engineering possible in experiments which is important to the understanding of these properties. In this article, we report the first principles atomistic study of a-AlGaN alloys. The resultant a-AlGaN band-gap variation with composition and the calculated bond length distribution are in good agreement with available experiments. Another interesting result is that these amorphous materials, unlike other amorphous systems or glasses which look locally very similar to the crystal, apparently have local environments very different from the main crystalline morphology. This is odd and interesting, probably associated with the ionicity of the materials. The current work provides insight into the characteristics of geometry, bonding, defects, electronic structures, electronic localization, and dynamics of a-AlGaN alloys.

The article is organized as follows: The computational approach is described briefly in Sec. II; the construction of the structural model is presented in Sec. III; the geometrical properties of pair correlation functions, coordinations, ring statistics, angular distributions, and bond lengths are given in Secs. IV A, IV B, IV C, and IV D, respectively. In Sec. V, the electronic properties of density of state, electronic localization, and dependence of band gap on Al composition will be discussed. Results for dynamical properties are given in Sec. VI. Finally, conclusions are summarized in Sec. VII.

[a]Electronic mail: kuiying.chen@nrc.ca

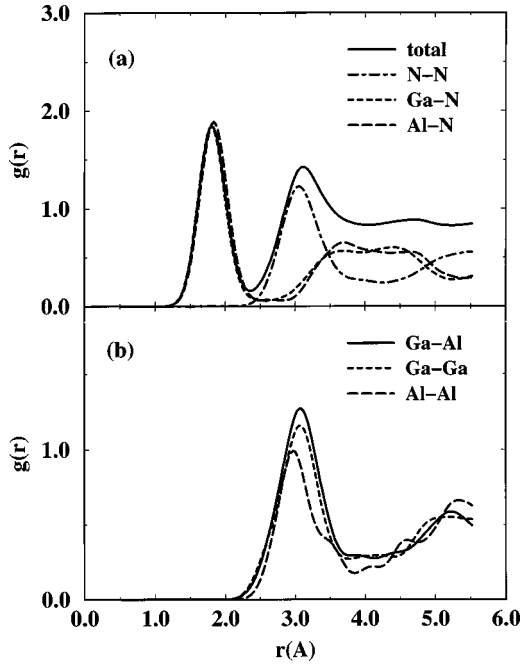

FIG. 1. Pair distribution functions (PDFs) $g(r)$ of a-$Al_{25}Ga_{75}N$ alloy. (a) The total in the figure represents the total PDF. N–N, Ga–N, and Al–N, throughout the article, represent the PDFs of N–N, Ga–N, and Al–N correlations, respectively. (b) Ga–Al, Ga–Ga, and Al–Al represent partial PDFs of Ga–Al, Ga–Ga, and Al–Al correlations.

II. THEORY

We applied an approximate self-consistent first principles multicenter tight-binding molecular dynamics approach based on density functional theory within the local density and norm-conserving nonlocal pseudopotential approximations.[22,23] The basis functions are slightly excited pseudo-atomic-orbitals with confinement radii of 5.4 a_B for both Al and Ga, and 4.0 a_B for N, respectively.[28] The exchange-correlation functional used is the Ceperley–Alder form.[24] In our calculations, the minimal basis with one *s* and three *p* orbitals was employed per site. This approach has been extensively applied in the calculation of amorphous alloys[25–27] and reproduces all the essential features of band structures of wurzite (WZ) and zincblende (ZB) of GaN and AlN (Ref. 28) in the near band gap in agreement with more accurate LDA calculations.[29]

III. MODEL

We constructed five initially random 216-atom models for $Al_xGa_{1-x}N$ alloys, with the Al fraction x being 0%, 25%, 50%, 75%–100%, respectively. Both experimental and theoretical investigations confirm that the lattice constants of $Al_xGa_{1-x}N$ alloys vary in a linear relation with the alloy composition.[30,31] By reducing the alloy density for each composition step by step, we can get the density of amorphous $Al_xGa_{1-x}N$ by minimizing the total energy with respect to the unit cell volume. For each cell, the first 4.4 ps molecular dynamics simulations were performed for the initial random configuration at the temperature of 10^4 K. The network was then equilibrated at 8×10^3 K and then 6×10^3 K, each for 2.2 ps, respectively. The average force is around 4.0 eV/Å.

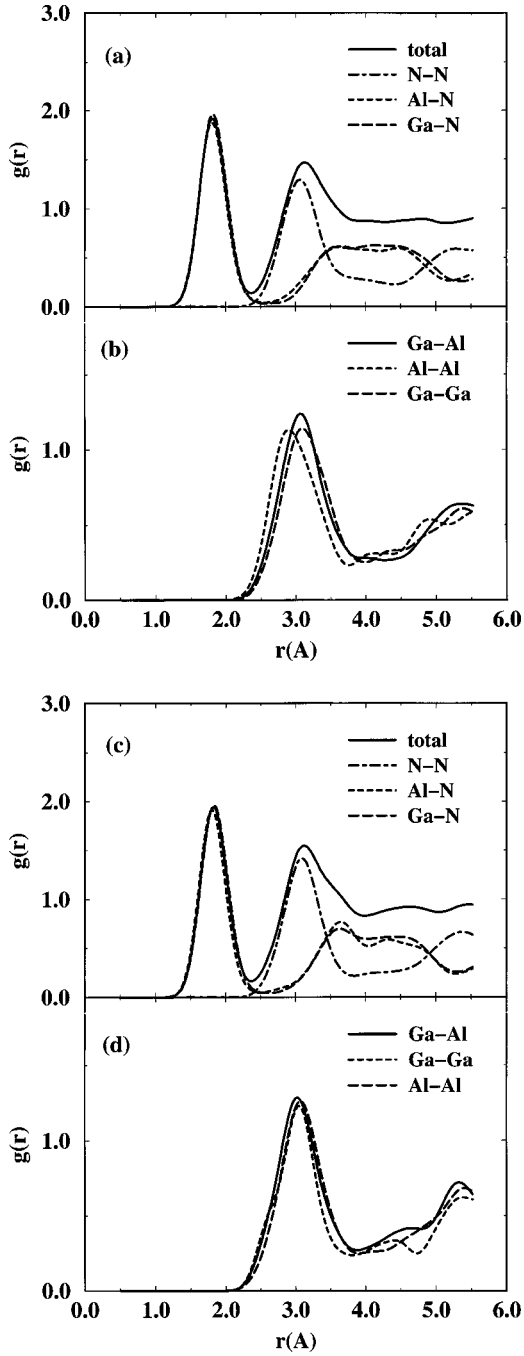

FIG. 2. (a) and (b) are the PDFs of a-$Al_{50}Ga_{50}N$ alloy; (c) and (d) are PDFs of a-$Al_{75}Ga_{25}N$ alloy.

Finally slow dynamical quenching was performed to fully relax the system to zero temperature (atoms in zero-force positions). The simulation was done at a constant volume and only the Γ point to sample the Brillouin zone was used. Charge transfer was calculated self-consistently in the simulations, which is essential in modeling these significantly ionic materials.

IV. ATOMIC STRUCTURAL PROPERTIES

A. Pair correlation functions

The resultant topological disorder of a-$Al_xGa_{1-x}N$ alloys has been described by pair correlation function. The

total and partial pair correlation functions $g(\mathbf{r})$ and $g_{\alpha\beta}(\mathbf{r})$ are defined as in the same manner as those of[32]

$$g_{\alpha\beta}(\mathbf{r}) = c_\beta \Omega_0 N_\alpha^{-1} \left\langle \sum_{i,j} \delta(\mathbf{r} + \mathbf{R}_i^\alpha - \mathbf{R}_j^\beta) \right\rangle, \quad (1)$$

where the c_β is the composition of the β-type element, the $\mathbf{R}_i^\alpha (i = 1,2,-,N_\alpha)$ are the positions of the α-type atoms. The summations are over all atoms in the supercell, and are restricted to $i \neq j$ when $\alpha = \beta$; Ω_0 is the volume of the system. When disregarding the type of atoms, Eq. (1) can yield the total correlation function $g(r)$. According to the first nearest neighbor peak in the pair correlation function, the average bond length is easily determined, and the average coordination radii of atoms are calculated within the first minimum of $g(r)$. The same method can be used to examine local coordinations, ring statistics.

The topology of the resultant networks was analyzed using pair correlation functions. To our knowledge, the pair correlation function has not been experimentally determined for a-$Al_xGa_{1-x}N$ alloys. In all compositions of a-$Al_xGa_{1-x}N$ alloys, a well defined nearest neighbor peak and a rapid loss of the interatomic correlation were observed, indicating the networks are topologically disordered. The character of pair correlation function of a-GaN in our 216-atom model is quite similar to our previous 64-atom model.[33] No homonuclear bonds (wrong bonds) are formed.

The pair correlation functions of a-$Al_{25}Ga_{75}N$ alloy are plotted in Fig. 1. It is evident from the total $g(r)$ that the first sharp peak is due to the Al–N and Ga–N partial correlations, while the second broaden peak comes from the N–N, Al–Al, Al–Ga, and Ga–Ga partial correlations. The contributions to the second peak from the Al–N and Ga–N partial correlations, however, are small. The locations of the bond lengths for Ga–N and Al–N pairs in Fig. 1(a) are determined as 1.83 and 1.80 Å, respectively, in which the Ga–N bond length is a bit longer than that of Al–N bond length. In a ternary a-AlGaN alloy, there is a correlation between Ga and Al atoms. It is interesting to note from Fig. 1(b) that the correlation between the distinguished metal Ga and Al atoms (Ga–Al pair, e.g., the tendency to form this bond) is a little stronger than that of any Ga–Ga or Al–Al pair. The separations among N–N, Ga–Ga, Ga–Al, and Al–Al correlation pairs are determined to be approximately 3.05, 3.05, 3.06, 2.96Å, respectively, which is in good agreement with recent extended x-ray absorption fine structure (EXAFS) measurements.[34] It was remarkable that no bonds formed between cation or anion pairs within the first shell. As in a-GaN alloy, no wrong bonds are formed due to ionicity. The short-range order of a-$Al_{25}Ga_{75}N$ model can be essentially characterized as each cation atom being surrounded solely by anion atoms.

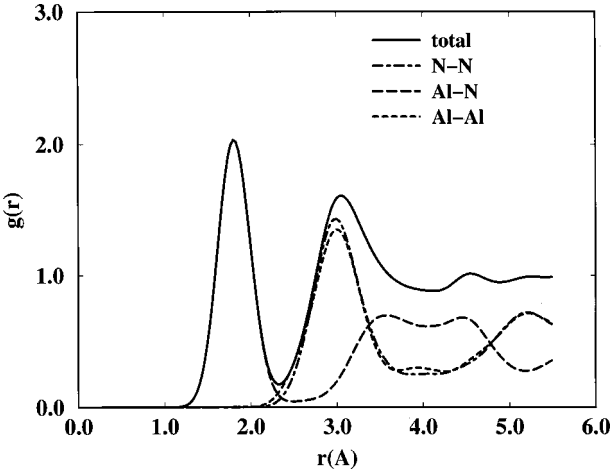

FIG. 3. PDFs for a-AlN.

Figures 2(a) and 2(b) illustrate the pair correlation functions of a-$Al_{50}Ga_{50}N$ alloy. As shown in Fig. 1(a), the partial correlation functions of both $g_{\mathrm{AlN}}(r)$ and $g_{\mathrm{GaN}}(r)$ behave similarly, especially before the first minimum after the nearest neighbor peak. It provides evidence that Ga atoms can be replaced by Al atoms without significantly altering the local structure. Figures 2(c) and 2(d) and 3 depict the pair correlation functions of a-$Al_{75}Ga_{25}N$ and a-AlN alloys. As expected, the $g(r)$ of a-$Al_{75}Ga_{25}N$ alloy is similar to the one of a-$Al_{25}Ga_{75}N$ alloy if we treat Ga as Al atom, and for a-AlN alloy, like in a-GaN alloy, no wrong bonds are formed.

B. Coordination and ring statistics

Based on the nearest neighbor distance determined in the preceding section, we can perform the local coordination and ring statistics analysis as summarized in Table I. It clearly shows that the number of threefold atoms, which plays a key role in the properties of a-$Al_xGa_{1-x}N$ alloys, decreases significantly from 147 (a-GaN) to 47 (a-AlN). The fraction of threefold coordination in a-AlN is only one third of that in a-GaN. It is known that the fourfold coordination reflects the structural character of crystalline GaN and AlN. Thus if we define a threefold coordination as a defect, then we will find that a-GaN is more *defective* than a-AlN. In other words, the

TABLE I. Summary of local coordination analysis in a-$Al_xGa_{1-x}N$ alloys. The threefold and fourfold columms represent threefold and fourfold coordinations, and the 4- ring and 6-ring represent threefold and fourfold ring statistics. N_{A-B} define the nearest neighbor coordination number of B atom around A atoms.

Alloys	Threefold	Fourfold	4 ring	6 ring	$N_{\mathrm{N-Al}}$	$N_{\mathrm{N-Ga}}$	$N_{\mathrm{Al-N}}$	$N_{\mathrm{Ga-N}}$
GaN	142	74	58	424		3.43		3.43
$Al_{25}Ga_{75}N$	114	102	103	503	0.90	2.54	3.59	3.43
$Al_{50}Ga_{50}N$	90	126	129	622	1.81	1.78	3.61	3.56
$Al_{75}Ga_{25}N$	64	152	144	847	2.80	0.91	3.72	3.63
AlN	47	164	163	1116	3.8		3.8	

degree of the order in a-$Al_xGa_{1-x}N$ alloys increases gradually from a-GaN, through a-AlGaN alloys, to a-AlN. The behavior of fourfold coordination follows, however, the inverse trend (74–126) if compared to the threefold one. The sixfold ring with the character of crystalline GaN and AlN behaves much similar to the fourfold coordination. Therefore, the local coordination and ring statistics supplement additional geometry information for our better understanding structural properties. It is interesting to observe fourfold rings which are not observed in either the crystalline GaN and AlN. Unlike the threefold coordination, the fourfold ring, however, increases with Al composition. The ratio of fourfold ring over sixfold ring coordination throughout a-$Al_xGa_{1-x}N$ alloys is around one fifth or even less.

The chemical short-range order (CSRO) is a well known feature of alloys, especially in the ionic materials. It is known that there are several different means to describe CSRO. In this article, we will use approaches based on the atomic geometry and electronic structural information to describe CSRO. First, we define N_{A-B} as the nearest neighbor coordination number of atom B surrounded by A atoms in an alloy. In a-GaN, $N_{Ga-N}=N_{N-Ga}=3.43$ is obtained. With the addition of Al atoms, for example, as in a-$Al_{25}Ga_{75}N$ alloy, $N_{N-Al}=0.90$ is gained. The N_{N-Ga} is then reduced to 2.55. In addition, it is shown that $N_{Al-N}=3.594>N_{Ga-N}=3.432$ is held, although Al composition takes only one third of Ga component. It reveals that the CSRO due to Al is more significant than Ga.

For a-$Al_{50}Ga_{50}N$, we find that $N_{N-Al}=1.81>N_{N-Ga}=1.78$ and $N_{Al-N}=3.61>N_{Ga-N}=3.56$. It demonstrates that Al will induce more CSRO in the nitride alloys than by Ga. From $N_{N-Al}=2.80$ in a-$Al_{75}Ga_{25}N>N_{N-Ga}=2.547$ in a-$Al_{25}Ga_{75}N$, and $N_{Al-N}=3.72$ in a-$Al_{25}Ga_{75}N>N_{N-Al}=3.594>N_{Ga-N}=3.432$ in a-$Al_{25}Ga_{75}N$, we confirm the ionicty of Al–N bond is stronger than Ga–N. In a-AlN we have $N_{N-Al}=3.805=N_{Al-N}>N_{Ga-N}$ in a-GaN. This may be due to more threefold coordination in a-GaN than a-AlN.

C. Angular distribution

The topology of a-$Al_xGa_{1-x}N$ alloys consists of threefold and fourfold coordinated sites. The most significant angular distributions are those of the triads Al(Ga)–N–Al(Ga) and N–Al(Ga)–N for these strong ionic alloys. The ring statistics of structure will be helpful to interpreting the angular distribution. In our definition, the angle is assigned exclusively to the smallest ring as preceding analysis. An angle is assigned to its lowest order (threefold ring) on the assumption that these rings are relevant ones to the short order. We will determine angular distributions for all possible nearest-neighbor configurations.

In crystalline AlGaN alloys, only a small number of characteristic bond angles occur, the disordered alloys are characterized by broadened angular distributions. We calculated the angular distributions for Al(Ga)–N–Al(Ga) and N–Al(Ga)–N pairs. We examined the trend of angular distribution varying from a-GaN through the alloys to a-AlN. It is apparent that angular distributions of a-$Al_xGa_{1-x}N$ alloys are broadened compared to their crystalline counterparts.

For a-GaN alloy, there are several peaks as shown in Fig. 4(a), the most significant of those are at ~86°, 105°, 111°, and 115° for angle N–Ga–N. There is only one main peak of 117° for the Ga–N–Ga angle. The ring distributions reveal that fourfold rings, which are not observed in crystalline GaN, account almost entirely for the peak at 86°. The sixfold rings are the most significant ring structures (see Table I), and contribute to all the rest angle peaks above.

For a-$Al_{25}Ga_{75}N$ alloy, the angular distribution is presented in Fig. 4(b). Three main peaks at ~88°, 107°, and 115°, for angle N–Al(Ga)–N are observed. This is expected when one considers the result for the a-GaN alloy in the preceding section. The fourfold rings make a large contribution to the peak at 88°. The rest of the peaks are contributed by the sixfold rings. The angular distribution for Ga–N–Ga, unlike the one in pure a-GaN alloy (nearly centered at 117°), has several peaks at ~95°, 101°, 110°, 115°, and 121°, respectively. The angle peak 88° arises from the fourfold ring distribution. Similarly, the rest can be explained in terms of sixfold rings. The angle Al–N–Al has one peak centered at ~111°, which is not strong in strength probably due to the small component of Al composition.

For the a-$Al_{50}Ga_{50}N$ alloy, the angular distribution of N–Al(Ga)–N [Fig. 4(c)], similar to the result in the a-$Al_{25}Ga_{75}N$ alloy, has three subpeaks around 87°, 107°, and 114°, respectively. The angles of Ga–N–Ga and Al–N–Al, however, behave differently from the one in the a-$Al_{25}Ga_{75}N$ alloy. The main peak of Ga–N–Ga is located at ~113°, while the main peak of Al–N–Al is located at ~106°. Both peaks derive partly from the sixfold rings. Due to the equal fraction of Al and Ga, we observed that both angles of Ga–N–Ga and Al–N–Al have broader peaks around 88°, which can be explained in terms of distribution of fourfold rings.

In the case of the a-$Al_{75}Ga_{25}N$ alloy, we observed that the angles N–Al(Ga)–N and Al–N–Al nearly follow the same curves except for their subpeaks which are around 86° and 91°, respectively [Fig. 4(d)]. Both angles have two main peaks located around 105° and 115°. In addition, the angular distribution of N–Al(Ga)–N is slightly wider than that of Al–N–Al. It is also seen that the distribution of angle Al–N–Al in the a-$Al_{25}Ga_{75}N$ alloy is quite different from the angular distribution of Ga–N–Ga in the a-$Al_{25}Ga_{75}N$ alloy. The angular distribution of Ga–N–Ga in a-$Al_{75}Ga_{25}N$ behaves similar to Al–N–Al in the a-$Al_{25}Ga_{75}N$ alloy. For a-AlN, we find that angular distributions of both N–Al–N and Al–N–Al get close to each other [Fig. 4(e)], and the main peaks are well distributed around 109°, close to the main peak in crystalline AlN or GaN which dominated. In summary, the information from the angular distribution also suggests that the degree of order in a-$Al_xGa_{1-x}N$ alloys increases with the addition of Al composition.

D. Bond length distribution

By analysis of the pair correlation functions, we can calculate the average bond length for Ga–N and Al–N pairs of a-$Al_xGa_{1-x}N$ alloys. In addition, we can also determine the average distances of Ga–Ga and Al–Al pairs. Figure 5(a) depicts the average bond lengths for Ga–N and Al–N versus

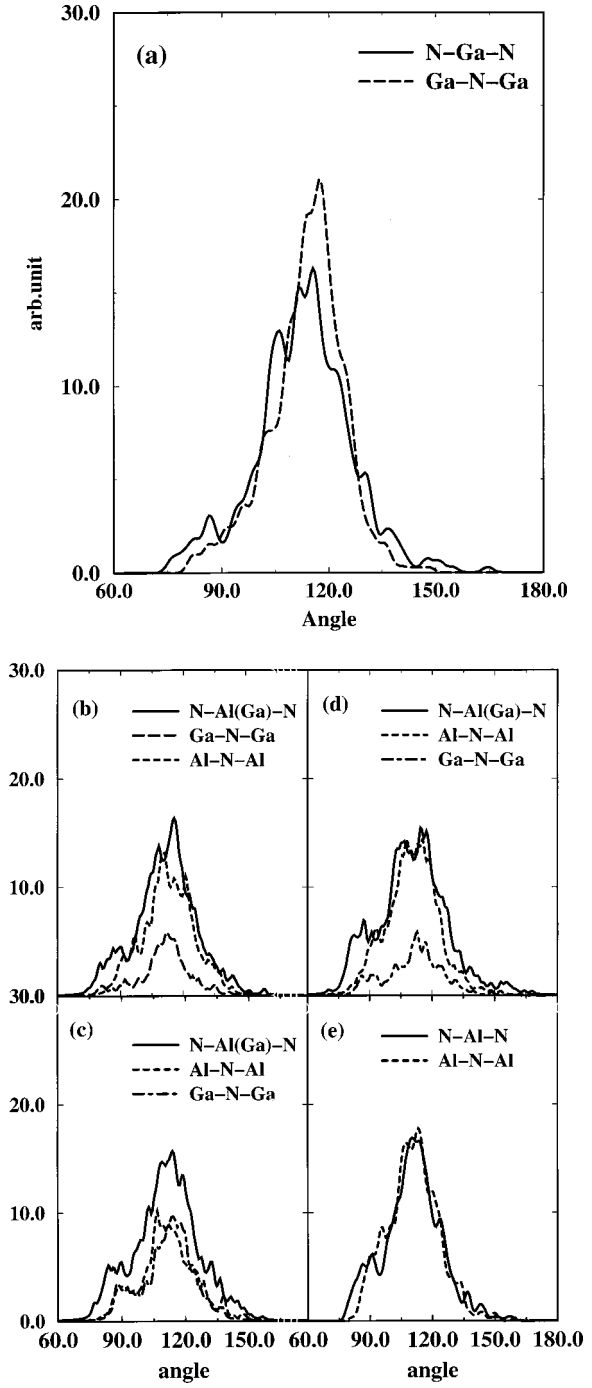

FIG. 4. (a) Angular distributions for *a*-GaN. The N–Ga–N and Ga–N–Ga represent the triad angles as described in the article; (b), (c), (d), and (e) are angular distribution functions of amorphous $Al_{25}Ga_{75}N$, $Al_{50}Ga_{50}N$, $Al_{75}Ga_{25}N$, and AlN.

Al composition. As can be seen, the variation of average bond lengths of both Ga–N and Al–N is small, and exhibits a nearly linear relation with Al composition. Figure 5(a) also demonstrates that the average bond length of Ga–N is a bit larger than that of Al–N throughout the alloy composition. Figure 5(b) shows the EXAFS experimental results of average bond lengths for both Ga–N and Al–N, the trend of average bond length variation is in agreement with calculations. The variation of lattice constant with Al content is associated with the small variations of the individual Ga–N and Al–N bond lengths, and is related to bond-angle distortions. In contrast to the small variation of the average bond length of Ga–N and Al–N, the average distance of both Ga–Ga and Ga–Al shown in Fig. 6(a), varies to some extent, which compares the EXAFS experiment with good agreement [Fig. 6(b)].

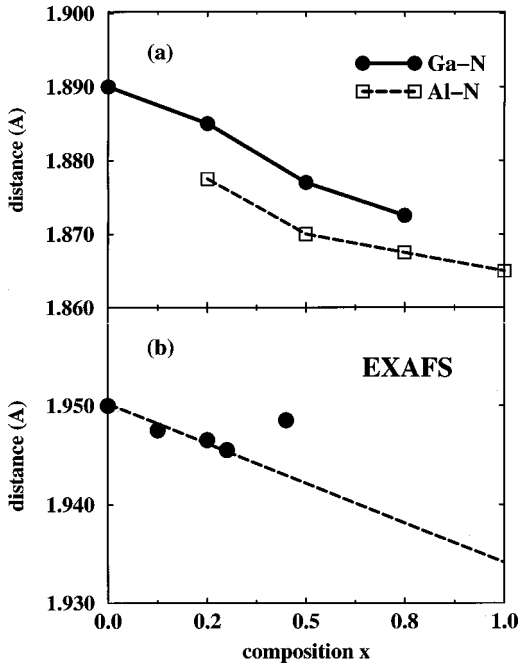

FIG. 5. (a) Calculated bond lengths of Ga–N and Al–N pairs vs Al composition; (b) the bond length of Ga–N pair given by EXAFS experiment.

V. ELECTRONIC STRUCTURE

A. Density of states

Electronic structure has been described by the electronic density of state (EDOS), which was obtained by summing suitably broadened Gaussians centered at each eigenvalue. Figure 7 shows the EDOS for a-$Al_xGa_{1-x}N$ alloys. The conduction band (CB) edges exhibit more tailing than the valence band (VB) edges. The VB edges, however, are insensitive to Al composition. It is quite remarkable that there are no electronic states in the band gap in the whole Al composition range. Therefore, no deep carrier traps exist, which is consistent with experimental observation. Based on the defect analysis in the preceding sections, it is found that the threefold coordinated defects show a strongly ionic sp^2 type of bonding.

B. Electronic localization

The nature of the band tail states in the amorphous system is of fundamental interest, and it is known that disorder induces localization of electronic states. The localization is determined by the microscopic structure of the band tail, the midgap eigenstates, and the dependence of this structure on the energy of the state. In this article, the electronic localization of band tail states is estimated by the inverse participation ratio (IPR) of

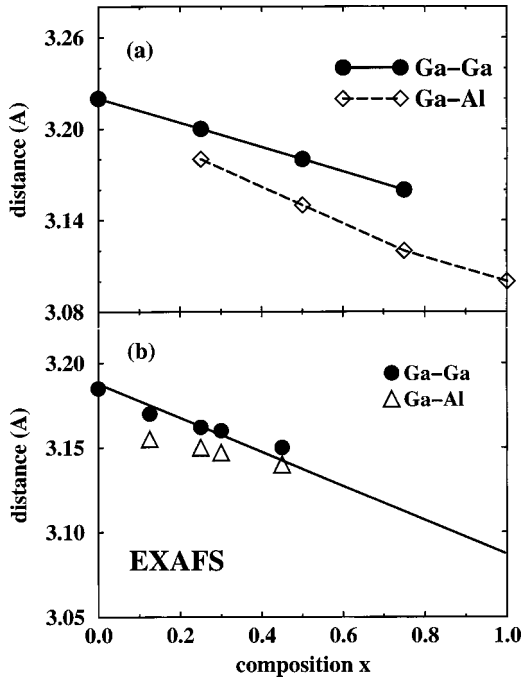

FIG. 6. (a) Calculated distance between Ga–Ga and Ga–Al pairs; (b) the distance between Ga–Ga and Ga–Al pairs given by EXAFS experiments.

$$q_2(\epsilon_i)=\sum_{n=1}^{N} q(n,\epsilon_i)^2, \tag{2}$$

where N and ϵ_i denote the number of atoms in the cell and the eigenvalue, respectively, and $q(n,E)$ is the Mulliken charge localized on atom site n in a certain eigenstate E. A completely localized state is described by $q_2=1$, and a completely delocalized state by $q_2=1/N$. The electronic localization of amorphous $Al_xGa_{1-x}N$ is illustrated in Fig. 8. By analysis of the electronic eigenvectors, we find that the band tail states, on either side of the Fermi level, are significantly localized. To differentiate between threefold and fourfold sites in amorphous configurations, the IPR is depicted in Fig. 9 for the a-$Al_{25}Ga_{75}N$ alloy. It is found that the localization of band tails are due mostly to threefold sites. This conclusion is valid for other alloy compositions. Figure 9 shows the localization of the eigenstate on N and Ga or Al sites. As can be seen, the VB states in a-$Al_xGa_{1-x}N$ alloys are most localized on threefold N sites, while the CB states are most localized on either the threefold Ga or Al sites. As the number of threefold defects in our first principles calculations goes down with increasing Al composition for five models, the electronic localization of band tail states is reduced, this can be seen by the reduction of IPR values shown in Fig. 8 so the conclusion about the degree of order of a-$Al_xGa_{1-x}N$

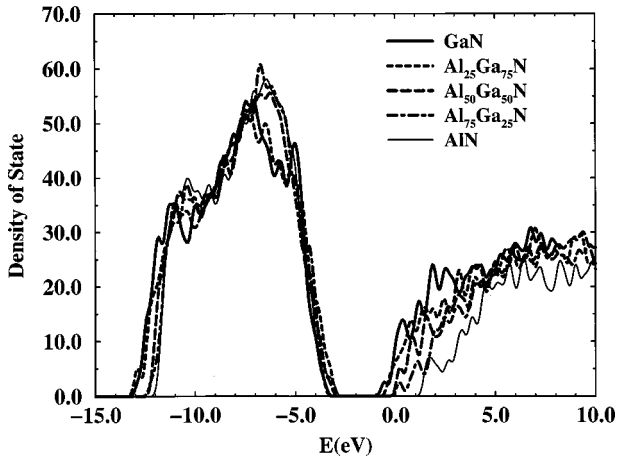

FIG. 7. Electronic density of state of a-$Al_xGa_{1-x}N$ alloys, in which the Al composition x being 0%, 15%, 50%, 75%, and 100%, respectively.

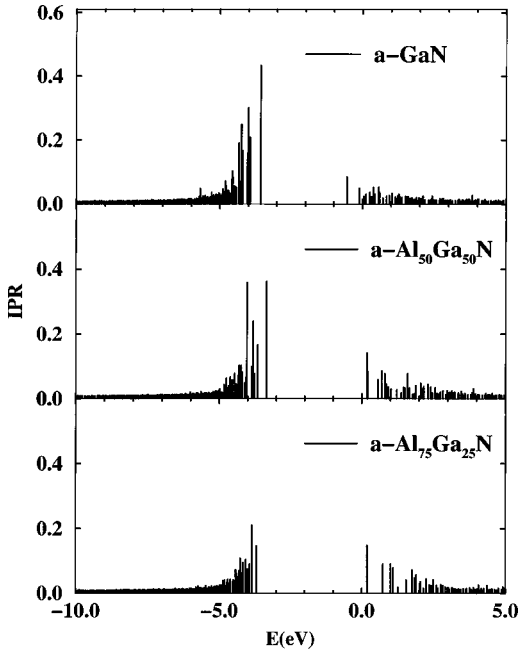

FIG. 8. Inverse partition ratio (IPR) of electronic localization for specifically chosen amorphous GaN, $Al_{50}Ga_{50}N$, $Al_{75}Ga_{25}N$.

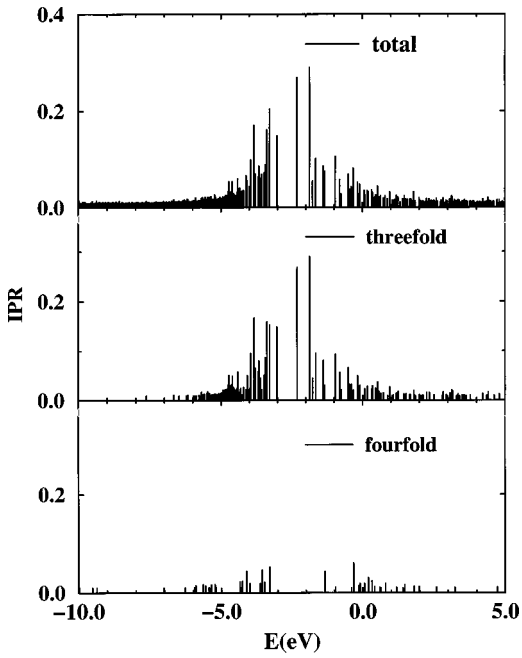

FIG. 9. Total IPR and its projection on threefold and fourfold sites in a-$Al_{75}Ga_{25}N$ alloy.

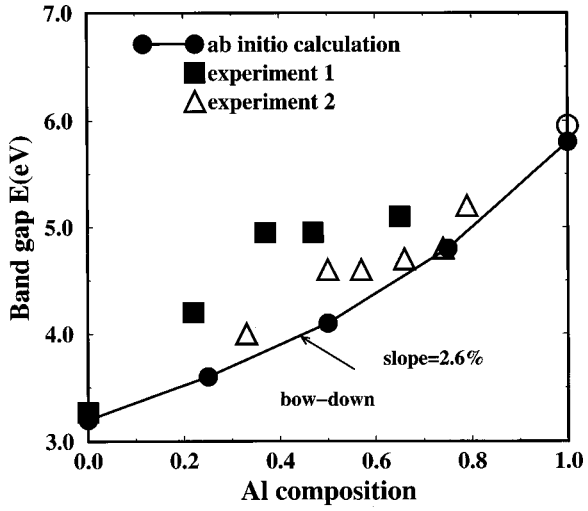

FIG. 10. Bandgap of a-$Al_xGa_{1-x}N$ alloys vs Al composition.

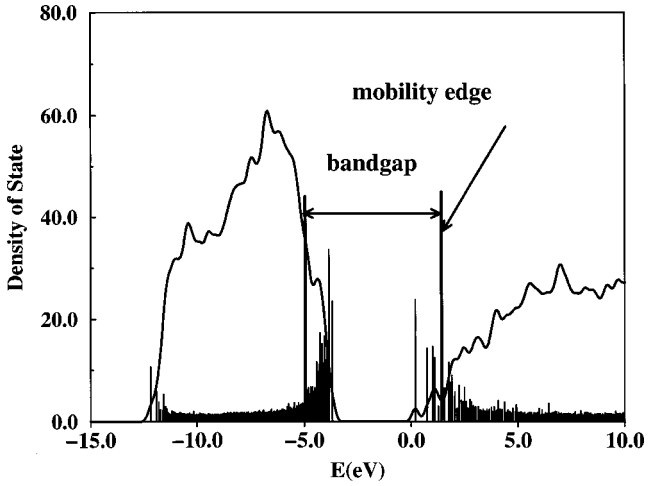

FIG. 11. Band-gap definition accepted in the article.

alloys from the electronic localization is consistent with the one by atomic geometry approaches like coordination and ring statistics analysis.

C. Dependence of band gap on composition

Figure 10 shows the dependence of band gap on composition of two sets of $Al_xGa_{1-x}N$ alloy film data versus x, the Al composition by both experimental and first principles calculations. It is shown that the band gap by theoretical calculations shows a small downward bowing behavior. The average slope of band gap by theoretical calculations is around 2.62, while the slope of band gap by experiment is around 2.68 so the calculated results are in good agreement with experiments. For our amorphous AlGaN alloys, we define the band gap as the difference between the mobility edge located at both conduction band and valence band edges (see Fig. 11). By this definition, we find that the calculated band gap is larger than the experiment by about the same amount of 1.4 eV for both end-point amorphous GaN and AlN which is consistent with recent first principles calculations of crystalline wurzite and random GaN and AlN.[21] In this article, for example, we found that the calculated band gaps for end-point amorphous GaN and AlN are 4.62 and 7.24 eV, respectively, while experimental results are 3.27 and 5.95 eV. The calculated results are 1.4 eV larger than the experiment for both end-point materials. This enables us to reliably calculate the variation of the electronic band-gap energy as the fraction of Al composition. In addition, Fig. 10 shows the theoretically calculated band gap shifted by 1.4 eV in the whole composition range.

VI. DYNAMICAL PROPERTIES

The dynamical properties of our models are analyzed with the vibrational density of state (VDOS), threefold and fourfold site projection of VDOS, and inverse participation ratio (IPR). The eigenvalues and eigenvectors are obtained from the dynamical matrix. The dynamical matrix is determined by displacing each atom with 0.03 Å in three orthogonal directions and then performing first principles force calculations for all the atoms for such displacement. Each calculation yields a column of force constant matrix. The vibrational eigenvectors and eigenvalues of the supercell are then obtained by diagonalizing the dynamical matrix. The VDOS was determined from the vibrational eigenvalues by summing Gaussians broadened form centered at each eigenvalues with a width of 120 cm^{-1}.

As discussed in the preceding section, the character of a-$Al_xGa_{1-x}N$ alloys involves mixed threefold (mixture of threefold sp^2 bonding) and fourfold (sp^3 bonding) coordinations. Figure 12 represents the VDOS of a-GaN, in which the threefold coordinations are the key structural components. It is evident that the VDOS shows double broadened peaks around 200 and 800 cm^{-1}, respectively. As in the a-GaN, there are many sp^2 bonding sites. We find that the VDOS of a-GaN has double peaks in the energy region between 200 and 800 cm^{-1}. Probably due to the mixture of three- and fourfold bonding sites in a-GaN, the VDOS of a-GaN has no extra intensities beyond 800 cm^{-1}.

As known in a-$Al_xGa_{1-x}N$ alloys, the amount of sp^3 bonding increases while the sp^2 bonding decreases for increasing Al composition x, and the double peak behavior of VDOS has been reduced gradually as shown in Fig. 13. The geometrical analysis shows that most threefold sites are connected to the fourfold sites. They probably wash out the valley between two peaks, and only one main peak of VDOS exists in a-AlN.

In order to get further insight into this problem, we performed detailed analysis for the local VDOS by focusing on the projection of VDOS on all threefold and fourfold sites. As an example, we plot the site projection of VDOS for a-GaN. As one can see, neither the threefold site nor the fourfold site of VDOS can represent the main character of the total VDOS of a-GaN. It appears that the mixture of bonds between threefold and fourfold sites in alloys produce new vibrational states which are absent in the pure threefold or fourfold network. This behavior becomes even more obvious when the energy is beyond 1000 cm^{-1}, in that region the VDOS of pure threefold and fourfold sites disappears. It is useful to compare the trend of threefold-VDOS versus Al composition as shown in Fig. 14(a). As expected, the

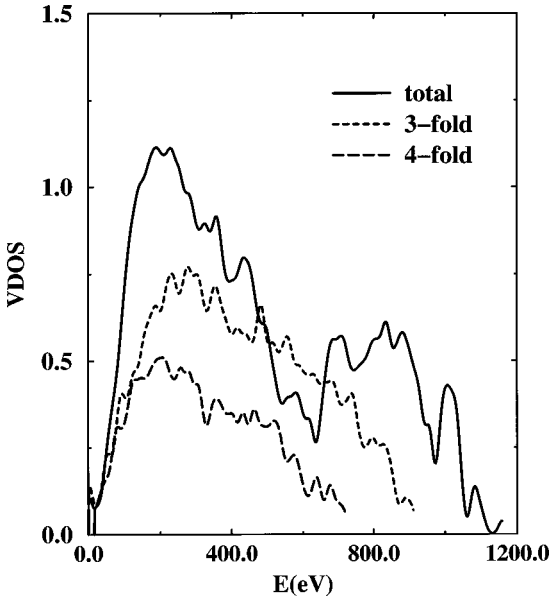

FIG. 12. Vibrational density of state (VDOS) of *a*-GaN. The threefold and fourfold represent the projection of VDOS on threefold and fourfold sites in *a*-GaN.

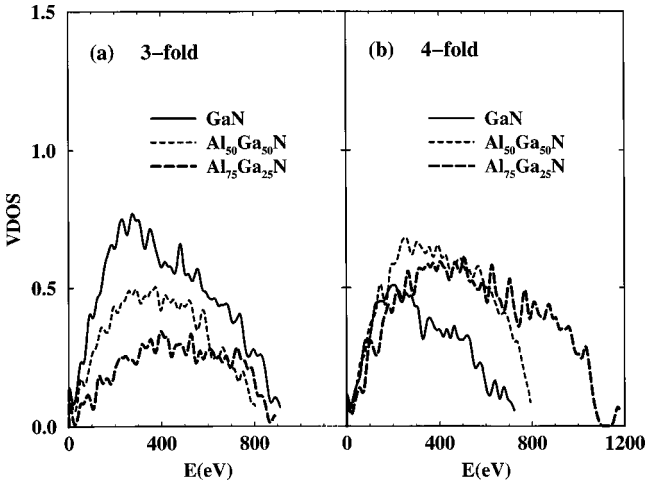

FIG. 14. (a) and (b) represent trends of VDOS projection on threefold and fourfold sites vs composition.

strength of threefold-VDOS is reduced gradually with the addition of Al, and the main peak position of threefold-VDOS moves towards the high energy region. Similarly, Fig. 14(b) shows the fourfold-VDOS versus Al. Contrary to Fig. 14(a), we find that the strength of fourfold-VDOS increases, and still shows intensities at high energy region.

The degree to which each vibrational mode is either localized or extended in nature can be characterized by its inverse participation ratio, defined for each mode as $P^{-1}=\Sigma_j(\mathbf{u_j}\cdot\mathbf{u_j})^2(\Sigma_j\mathbf{u_j}\cdot\mathbf{u_j})^{-2}$, where $\mathbf{u_j}$ is the vibrational eigenvector ($j=1,2-,N$; N being the number of atoms in the system). The spatially extended modes have a small value of P^{-1}, of the order of $1/N$, whereas localized modes have a larger ratio that can reach a maximum value of 1 for a mode completely localized on a single atom. As an example of localization of VDOS, we plot IPR for *a*-GaN and *a*-$Al_{50}Ga_{50}N$ in Fig. 15. It is apparent that the vibrational modes below 1000 cm^{-1} are extended, and then become more and more localized at higher frequencies. From Fig. 15 we also find that weakly localized states are around 600 cm^{-1} for *a*-GaN, and correspond to the valley position of VDOS for *a*-GaN.

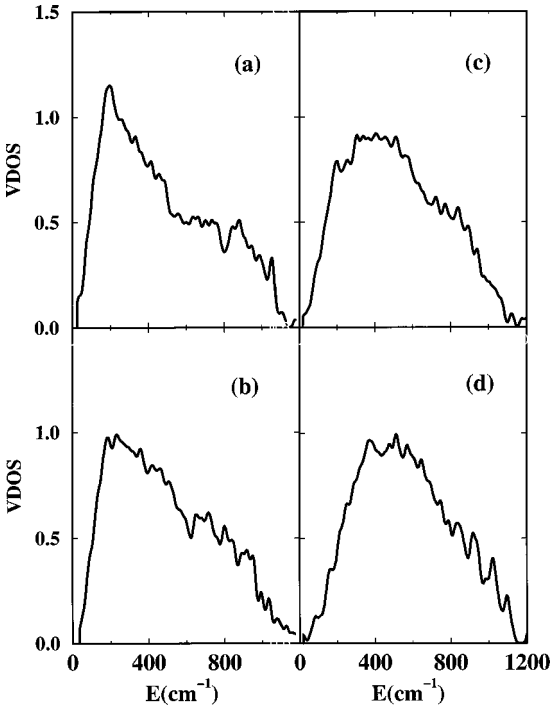

FIG. 13. VDOS of (a) *a*-$Al_{25}Ga_{75}N$, (b) *a*-$Al_{50}Ga_{50}N$, (c) *a*-$Al_{75}Ga_{25}N$, and (d) *a*-AlN.

VII. CONCLUSIONS

In this study, we reported structural models of *a*-$Al_xGa_{1-x}N$ alloys constructed with first principles molecular dynamics techniques. The simulation of these materials suggests that the coordination of both cation and anion sites is remarkably variable, and implies that the amorphous III-N alloys are quite different structurally and electronically from their crystalline counterparts. Despite these significant differences, the amorphous networks never exhibit deep electronic traps and have large gaps with moderate bandtailing. These materials have proven utility as a host for rare-earth photonic devices and the robust lack of midgap states suggests their possible exploitation as an electronic material. Clearly the latter goal is far from certain, but these amorphous wide gap materials have special advantages: (1) a natural tendency to a state free gap without hydrogenization, a situation quite different from that for Si or diamond, and (2) these materials might be able to accommodate growth on a variety of substrates. As a final note, our work offers another hint about the surprising effectiveness of crystalline III–N materials in the presence of defects. In a crude sense our amorphous nitrides are exceedingly defective (from the perspective of the crystalline phases); yet even here there is a wide clean gap. It leads us to speculate that even in the

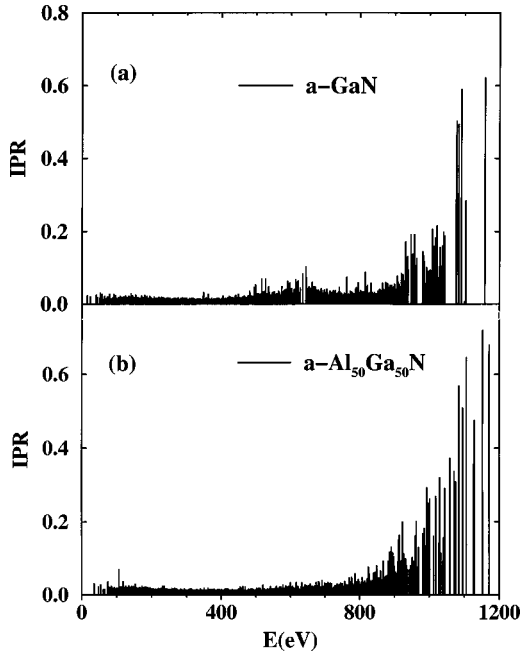

FIG. 15. IPR of VDOS for sample amorphous GaN and $Al_{50}Ga_{50}N$ alloys.

crystalline systems there may be remnants of the amorphous phases and at least optically, would not be easily differentiated from the crystal.

ACKNOWLEDGMENT

This work was funded by the Office of Naval Research through Grant Nos. N00014-99-1-0975 and NSF DMR 00-81006.

[1] W. C. Johnson, J. B. Parsons, and M. C. Crew, J. Phys. Chem. **36**, 2561 (1932).
[2] H. P. Maruska and J. J. Tietjen, Appl. Phys. Lett. **15**, 327 (1969).
[3] M. R. H. Kahn, Yoide, H. Itoh, N. Sawaki, and I. Akasaki, Solid State Commun. **60**, 509 (1986).
[4] M. J. Paisley, Z. Sitar, J. B. Posthill, and R. F. Davis, J. Vac. Sci. Technol. A **7**, 701 (1989).
[5] T. Lei, T. D. Moustakas, R. J. Graham, Y. He, and S. J. Berkowitz, J. Appl. Phys. **71**, 4933 (1992).
[6] T. Lei, M. Fanciulli, R. J. Molnar, T. D. Moustakas, R. J. Graham, and J. Scanlon, Appl. Phys. Lett. **95**, 944 (1991).
[7] Z. Sitar, M. J. Paisley, J. Rnan, J. W. Choyke, and R. F. Davis, J. Mater. Sci. Lett. **11**, 261 (1992).
[8] S. C. Jain, M. Willander, J. Narayan, and R. Van Overstraeten, J. Appl. Phys. **87**, 965 (2000).
[9] S. Bloom, G. Harbeke, E. Meier, and I. B. Ortenburger, Phys. Status Solidi B **66**, 161 (1974).
[10] P. E. Van Camp, V. E. Van Doren, and J. T. Deverse, Phys. Rev. B **44**, 9056 (1991).
[11] A. Munoz and K. Kunc, Phys. Rev. B **44**, 10372 (1991).
[12] A. Rubio, J. L. Corkill, M. L. Cohen, E. L. Shirley, and S. G. Louie, Phys. Rev. B **48**, 11810 (1993).
[13] A. F. Wright and J. S. Nelson, Phys. Rev. B **50**, 2159 (1994).
[14] A. Rubio, J. L. Corkill, and M. L. Cohen, Phys. Rev. B **49**, 1952 (1994).
[15] W. J. Fan, M. F. Li, T. C. Chong, and J. B. Xia, J. Appl. Phys. **79**, 188 (1996).
[16] E. A. Albanesi, W. R. L. Lambrecht, and B. Segall, Phys. Rev. B **48**, 17841 (1993).
[17] B. K. Agrawal, S. Agrawal, P. S. Yadav, and S. Kumar, J. Phys.: Condens. Matter **9**, 1763 (1977).
[18] H. Schulz and K. H. Thiemann, Solid State Commun. **23**, 815 (1977).
[19] Y. Koide, H. Itoh, N. Sawaki, I. Akasaki, and M. Hashimoto, J. Electrochem. Soc. **133**, 1956 (1986).
[20] H. Chen, K. Chen, D. A. Drabold, and M. E. Kordesch, Appl. Phys. Lett. **77**, 1117 (2000).
[21] J. Fritsch, O. F. Sankey, K. E. Schmidt, and J. B. Page, J. Phys.: Condens. Matter **11**, 2351 (1999).
[22] O. F. Sankey and D. J. Niklewski, Phys. Rev. B **40**, 3979 (1989).
[23] A. A. Demkov, J. Ortega, O. F. Sankey, and M. P. Grumbach, Phys. Rev. B **52**, 1618 (1995).
[24] D. M. Ceperley and G. J. Alder, Phys. Rev. Lett. **45**, 566 (1980).
[25] D. A. Drabold, P. A. Fedders, S. Klemm, and O. F. Sankey, Phys. Rev. Lett. **67**, 2179 (1991).
[26] P. A. Fedders, Y. Fu, and D. A. Drabold, Phys. Rev. Lett. **68**, 1888 (1992).
[27] M. Cobb, D. A. Drabold, and R. L. Cappelletti, Phys. Rev. B **54**, 12162 (1996).
[28] P. Stumm and D. A. Drabold, Phys. Rev. Lett. **79**, 677 (1997).
[29] E. A. Albanesi, W. R. L. Lambrecht, and B. Segall, Phys. Rev. B **48**, 17841 (1993); W. R. L. Lambrecht and B. Degall, in *The Properties of III-Nitrides*, edited by J. H. Edgar (INSPEC, London, 1994).
[30] D. K. Wickenden, W. A. Bryden, T. J. Kistenmacher, P. F. Bythrow, and K. Strohbehn, Johns Hopkins APL Tech. Dig. **16**, 246 (1995).
[31] Y. Koide, H. Itoh, M. R. Khan, K. Hiramatsu, N. Sawaki, and I. Akasaki, J. Appl. Phys. **61**, 4540 (1987).
[32] Y. Waseda, *The Structure of Non-Crystalline Materials* (McGraw-Hill, New York, 1980).
[33] M. Yu and D. A. Drabold, Solid State Commun. **108**, 413 (1998).
[34] K. E. Miyano, J. C. Woicik, L. H. Robins, C. E. Bouldin, and D. K. Wickenden, Appl. Phys. Lett. **70**, 2108 (1997).